Sulfur-Mediated Synthesis of Spherical Nickel Nanoparticles in a Chemical Vapor Reactor

Yong-Su Jo, Mansurbek Abdullaev, Gwang-Hwa Jin, Bhabani Sankar Swain, Byongpil Lee, Hyung-Sub Eom, Seok-Hong Min, Seok Ki Kim,* Young Keun Kim,* and Seung-Min Yang*

| ACCESS | | Metrics & More | | Article Recommendations | | Supporting Information |

ABSTRACT: In this study, we investigated the effect of the sulfur content in the $NiCl_2$ precursor on the shape of nickel nanoparticles (Ni-NPs) prepared by chemical vapor synthesis. We obtained spherical Ni-NPs when using anhydrous $NiCl_2$ mixed with $NiSO_4$ or Na_2SO_4 with a molar ratio of 0.002 as precursors without changing any other process parameters whereas faceted Ni-NPs when using only anhydrous $NiCl_2$ as a precursor. First-principles calculations supported experimental results, which showed that $NiSO_4$-mixed $NiCl_2$ and Na_2SO_4-mixed $NiCl_2$ precursors favored the growth of spherical NPs.
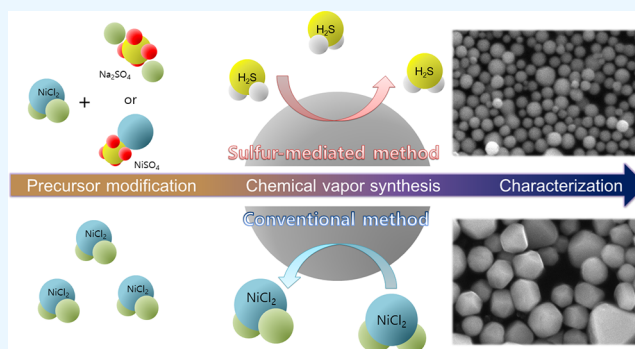
1. INTRODUCTION

Tuning the shape and size of nanoparticles is technologically important because macroscopic properties of NPs depend on their shape and size.[1−8] Enhancement of magnetic properties or catalytic activity by changing the shape of NPs has been reported.[9,10] Ni-NPs are most often used as electrode materials for multilayer ceramic capacitors (MLCCs). If the packing density of Ni-NPs is low when they are printed on the ceramic layer of MLCCs, then the porosity of electrodes will be high, and it may result in short circuits. If cubic NPs are ideally well-arranged, a higher packing density than spherical NPs can be achieved, but this is difficult due to their poor flowability.[11] Therefore, spherical NPs with a good flowability are preferred over cubic for electrode materials.

Several synthetic methods such as wet chemical synthesis[12] and vapor-phase synthesis[13−17] have been used for the preparation of Ni-NPs. For MLCC applications, highly crystalline Ni-NPs prepared by vapor-phase synthesis (VPS) such as chemical vapor synthesis (CVS)[13−15] and physical vapor synthesis (PVS) are preferred. Therefore, highly crystalline Ni-NPs are preferably synthesized via high-temperature processes such as chemical vapor synthesis (CVS)[13−15] and physical vapor synthesis (PVS).[17,18] CVS possesses an advantage over PVS in that it is easy to synthesize a narrow particle size range of NPs. The commonly employed approach is to synthesize Ni-NPs via thermal reduction of $NiCl_2$ in a reducing atmosphere, and the commonly observed shape of NPs is cubes or truncated cubes. This occurs because the equilibrium crystal shape of Ni nanocrystals favors the (100) crystal plane by selective adsorption of $NiCl_2$ on (100) in the

CVS process.[14,19,20] During particle formation, $NiCl_2$ vapor is adsorbed on the surface of the Ni-NPs and forms a cubic shape by lowering the surface energy of a specific surface. Therefore, a rapid reaction must be induced to prevent the formation of cubic structures.[14] A fast reaction and short residence time of NPs in CVS can be used to obtain spherical nickel. However, the process window is narrow, which inevitably acts as a constraint during the scale-up. Therefore, we attempted to synthesize spherical particles by adding the nonpreferential-adsorption type of impurity to the surface of Ni, which could destabilize the nanocrystal facet and strategically tune the shape of the Ni-NPs.[21,22]

It is necessary to manipulate selective impurities that can alter the adsorption properties such as the surface energy and surface anisotropy of Ni. We chose sulfur among the various elements that are adsorbed nonpreferentially on the Ni surface and cause a sintering delay effect that can eliminate the defects in MLCCs.[23,24] H_2S is a suitable candidate for the easy adsorption of S to Ni.[25,26] However, H_2S is toxic and dangerous for direct use in CVS. To overcome this problem, a suitable chemical that can locally produce H_2S in a CVS reactor would be highly beneficial for controlling the shape of

the Ni-NPs. We chose $NiSO_4$ and Na_2SO_4 as additives to realize our strategy to synthesize spherical Ni-NPs.

In this study, we carefully analyzed the impurity content of the initial $NiCl_2$ precursor to strategically modify the sulfur concentration of $NiCl_2$ in the precursor to be used. Toward this end, we prepared $NiSO_4$-mixed $NiCl_2$ and Na_2SO_4-mixed $NiCl_2$ precursors via spray-drying and used them to synthesize spherical Ni-NPs. We observed that the Na_2SO_4-mixed $NiCl_2$ precursor offered better results than $NiSO_4$-mixed $NiCl_2$ in terms of particle size distribution and the agglomeration ratio.

2. METHODS

2.1. Synthesis of Ni-NPs Using the $NiCl_2$ Precursor. A vertical hot-wall CVS reactor was used to prepare Ni-NPs with a fixed heating zone temperature of 1000 °C.[15] A schematic of the CVS reactor used in our experiments is shown in Figure S1. Nickel chloride hexahydrate ($NiCl_2 \cdot 6H_2O$, 97%, Research Institute of Industrial Science & Technology) was used as a precursor for the synthesis of Ni-NPs. The composition of the initial $NiCl_2$ precursor is listed in Table S1. Anhydrous $NiCl_2$ was prepared by spray-drying (B-290, Buchi) and vacuum-drying $NiCl_2 \cdot 6H_2O$. The prepared $NiCl_2$ precursor was injected into the CVS reactor using a powder feeder (ROVO, Fine Technics) with N_2 (99.9%) carrier gas at a flow rate of 34.09 standard liters per minute (SLM) (sample 1). H_2 reducing gas was flown separately into the reactor at a flow rate of 1 SLM into the particle formation zone, as shown in the schematic of the CVS reactor (Figure S1).

2.2. Synthesis of Ni-NPs Using $NiCl_2$ with S Additives. We used nickel sulfate hexahydrate ($NiSO_4 \cdot 6H_2O$, Sigma Aldrich, 98%) and sodium sulfate (Na_2SO_4, Sigma Aldrich, 99%) as additives for the synthesis of Ni-NPs. We prepared anhydrous $NiSO_4$-mixed $NiCl_2$ and Na_2SO_4-mixed $NiCl_2$ precursors by spray-drying and vacuum-drying. The details of the process parameters, such as the molar ratio, feed rate, and flow rate, for the synthesis of Ni-NPs are summarized in Table 1. We collected Ni-NPs from a powder collector connected to the reactor outlet and characterized them using the methods described in the following section.

Table 1. Process Parameters

sample number	feeding rate of the precursor (g/h)	molar ratio		total flow rate (LPM)
		$M_{Na_2SO_4}/M_{NiCl_2}$	M_{NiSO_4}/M_{NiCl_2}	
1	80.00			35.09
2	80.00		0.002	35.09
3	80.00	0.002		35.09

2.3. Characterization. The shape and size of the as-synthesized Ni-NPs were analyzed by field-emission scanning electron microscopy (FESEM, Quanta 250 FEG, FEI) after Au-Pd thin-film coating by sputtering. Additionally, more detailed shape and elemental mappings were analyzed using a field-emission high-resolution transmission electron microscope (HRTEM, JEM F200, TFEG). The geometric standard deviation (GSD) and the count median diameter (CMD) of Ni-NPs were determined via image analysis considering 200 particles. The agglomeration ratio was calculated by dividing the number of primary particles constituting the agglomerate by the sum of the primary particles constituting the agglomerate and nonagglomerating particles, which was

obtained through image analysis of more than 500 particles. The details of the calculation methods are described in eqs 1−3 in the SI. The phase and crystallinity of the Ni-NPs were analyzed using X-ray diffraction (XRD, Empyrean, PANalytical) with Cu Kα radiation in the $2\theta/\theta$ scan mode with a step size of 0.013°. Elemental analysis was performed using X-ray fluorescence (XRF; M4 TORNADO, Bruker) with an excitation energy of 0−10 keV.

2.4. Computational Methods. All density functional theory (DFT)[27] calculations were performed using the Vienna ab initio simulation package (VASP).[28,29] The electronic structure was described using the Perdew (Burke)−Ernzerhof exchange−correlation function within a generalized gradient approximation and projector-augmented wave pseudopotentials with a cutoff energy of 400 eV.[29−31] The conjugate gradient method was implemented to optimize the geometry, and the criteria for the convergence of energy and force were set at 10^{-6} eV and 0.01 eV/Å, respectively.

To reflect the effect of adsorbates on particle shape formation, we performed calculations by introducing adsorbates with different surface coverages onto two low-Miller-index planes: Ni(100) and Ni(111). These facets were represented by slabs composed of four-layered (2×4) and (4×4) surface unit cells. The bottom two layers of the slab were fixed at their bulk-optimized positions, and the top two layers, including any adsorbates, were allowed to relax. A Monkhorst−Pack ($4 \times 4 \times 1$) k-point mesh grid was implemented for all facets to integrate the Brillouin zone. For all modeled surface facets, the vacuum thickness along the z-direction was set at 15 Å to avoid unintended interactions between the slabs.

Since the surface densities were different in the aforementioned facets, the surface coverage of an adsorbate on a facet was calculated based on its surface area, which was normalized to that of the most closely packed Ni(111). This normalization enabled consistent surface coverage among all facets, regardless of the number of actual adsorption sites.

The adsorption energy was calculated as follows:

$$E_{ads} = E_{system} - [E_{slab} + E_{adsorbate}] \quad (1)$$

where E_{system} is the total energy of the optimized system, E_{slab} is the total energy of the bare Ni slab, and $E_{adsorbate}$ is the total energy of the isolated adsorbate.

The corresponding surface energy at a certain coverage was obtained according to eq 2:

$$E_{surf} = \frac{E_{system} - nE_{ref} - E_{ads}}{2A} \quad (2)$$

where E_{ref} is the reference energy of the unit composition obtained from the bulk calculation, E_{ads} is the absolute sum of the adsorption energies of the intermediates at a given coverage, n is the number of unit compositions on the surface, and A is the surface area.

3. RESULTS AND DISCUSSION

Figure 1a,b shows the FESEM image and the particle size histogram of Ni-NPs prepared by CVS using an anhydrous $NiCl_2$ precursor (sample 1). The faceted crystals including cubes and polyhedrons were observed in sample 1. The GSD and CMD of sample 1 were 1.35 and 243 nm, respectively. Notably, no agglomeration of particles occurred. Figure 1c,d shows the FESEM image and the particle size histogram of Ni-
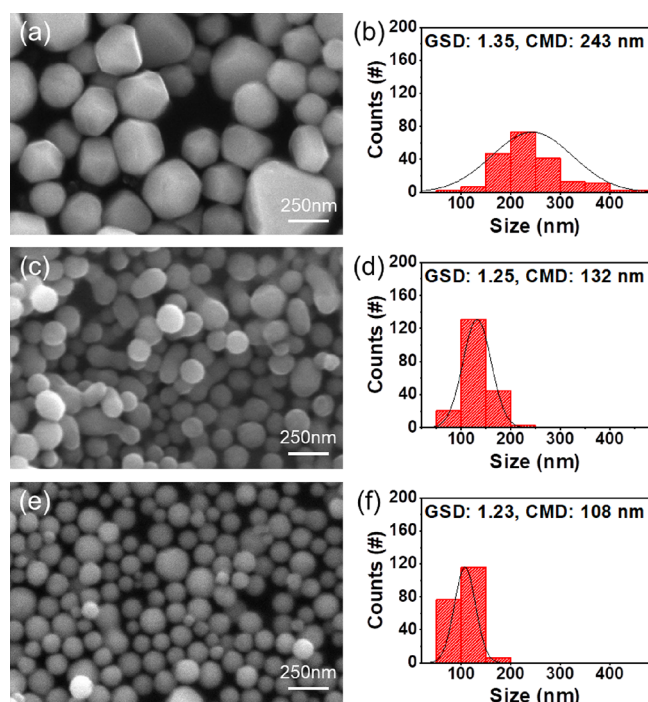
Figure 1. FESEM images and particle size histograms of Ni-NPs synthesized in the CVS reactor using different precursors; (a,b) $NiCl_2$, (c,d) $NiSO_4/NiCl_2$, and (e,f) $Na_2SO_4/NiCl_2$.

NPs prepared by CVS using the $NiSO_4$-mixed $NiCl_2$ precursor (sample 2). The GSD and CMD of sample 2 were 1.25 and 132 nm, respectively. The Ni-NPs in sample 2 were spherical with a smooth surface, but a few of them appeared to agglomerate. The calculated agglomeration ratio of sample 2 was 13.50%. Figure 1e,f shows the FESEM image and the particle size histogram of Ni-NPs prepared by CVS using the Na_2SO_4-mixed $NiCl_2$ precursor (sample 3). The GSD and CMD were 1.23 and 108 nm, respectively. Only spherical Ni-NPs were observed in sample 3, and the calculated agglomeration ratio of NPs in sample 3 was 4.34%. The calculated GSD, CMD, and agglomeration ratio data for samples 1−3 are summarized in Table 2, and low-magnification scanning electron micrographs of samples 1−3 are shown in Figure S2 in the SI.

Table 2. CMD, GSD, and Agglomeration Ratio of Ni-NPs Summarized for Ni-NPs Synthesized Using Different Precursors; Sample 1: $NiCl_2$, Sample 2: $M_{Na_2SO_4}/M_{NiCl_2} = 0.002$, Sample 3: $M_{NiSO_4}/M_{NiCl_2} = 0.002$

sample number	CMD (nm)	GSD	agglomeration ratio (%)
1	243	1.35	
2	132	1.25	13.50
3	108	1.23	4.34

Figure 2 panels (a and b), (d and e), and (g and f) show the high-resolution transmission electron microscopy (HRTEM) images of samples 1, 2, and 3, respectively. While only spherical Ni-NPs were observed in samples 2 and 3, various faceted crystals including cubes and polyhedrons were observed in sample 1. Figure 2 panels (c), (f), and (i) show selected-area electron diffraction (SAED) patterns of samples

1, 2, and 3, respectively. All patterns match face-centered cubic (FCC) Ni regardless of the particle shape.

Figure 3a−c shows EDS results of sample 1, where 99.99 wt % Ni and 0.01 wt % S were detected. Note that we did not add additional S to the precursor used in sample 1, but trace amounts of S were present as shown in Table S1. Figure 3d−f shows EDS results of sample 2, where 99.87 wt % Ni and 0.13 wt % S were detected. Figure 3g−j shows EDS results of sample 3, where 99.91 wt % Ni and 0.09 wt % S were detected. Na was added to the precursor used in sample 3, but it was difficult to quantify because it was present in small amounts.

Comparing the microstructures of Ni-NPs prepared by CVS using the three different precursors, it was observed that both $NiSO_4$-mixed and Na_2SO_4-mixed $NiCl_2$ precursors were more favorable for preparing spherical Ni-NPs than the pure $NiCl_2$ precursor. This confirmed that the formation of faceted Ni-NPs could be prevented by the intentional addition of S to the precursor. In addition, the agglomeration rate, which was 13.50% with $NiSO_4$-mixed $NiCl_2$, was reduced to 4.34% with Na_2SO_4-mixed $NiCl_2$. This will be discussed later in this section.

Figure 4 shows the XRD patterns of samples 1−3. The peaks appeared at 2θ = 44.5, 51.8, 76.4, 92.9, and 98.4° for the (111), (200), (220), (131), and (222) planes, respectively, of FCC Ni (JCPDS 04-0850). No peaks of residues or byproducts of the chemical reactions in the CVS were observed. The chemical reactions and their feasibility are explicitly discussed later in this section (eqs 1−9).

Figure 5 shows the XRF results for samples 1−3. The XRF results of sample 1 showed the presence of 99.60 wt % Ni and 0.40 wt % Cl. The Cl found in sample 1 might be a nonreacted $NiCl_2$ precursor that precipitated on the surface of the Ni-NPs.[14] In samples 2 and 3, Ni was expected along with Cl and S, as we used metal sulfate additives in our precursors. Because the intensities of S and Cl are relatively very small compared to that of Ni, a magnified view of the XRF data in the range of 2.0−3.5 keV is presented in the inset of Figure 5. We observed 98.65 wt % Ni, 1.33 wt % Cl, and 0.03 wt % S in sample 2 and 98.27 wt % Ni, 1.72 wt % Cl, and 0.01 wt % S in sample 3. The chemical compositions of samples 1−3 are summarized in Table 3.

Results indicated that metal sulfate as an additive in the $NiCl_2$ precursor enables the synthesis of spherical Ni-NPs in the CVS process. Moreover, Na_2SO_4 was found to be more beneficial than $NiSO_4$ in terms of its low agglomeration ratio. This is because NaCl, a byproduct of Na_2SO_4, inhibits agglomeration between particles owing to the previously reported in-flight coating.[15] However, we did not observe the presence of NaCl in the XRD and XRF results of sample 3. We assumed that NaCl was not observable because it is a very small and light molecule. Therefore, we investigated the effect of excessive Na_2SO_4 addition on the shape of Ni-NPs. The microstructure of Ni-NPs synthesized using a Na_2SO_4-mixed $NiCl_2$ precursor with a molar ratio of 0.02 is shown in Figure S3a,b. The XRD pattern of Ni-NPs synthesized using the Na_2SO_4-mixed $NiCl_2$ precursor with a molar ratio of 0.02 shows the $NiCl_2$ and NaCl phases in the sample (Figure S4). This byproduct was also confirmed by elemental analysis using XRF (Figure S5). As a result, we confirmed the formation of NaCl as a Na_2SO_4 byproduct, and we can conclude that a Na_2SO_4-mixed $NiCl_2$ precursor with a molar ratio of 0.002 provides an optimal amount of S for synthesizing spherical Ni-NPs.
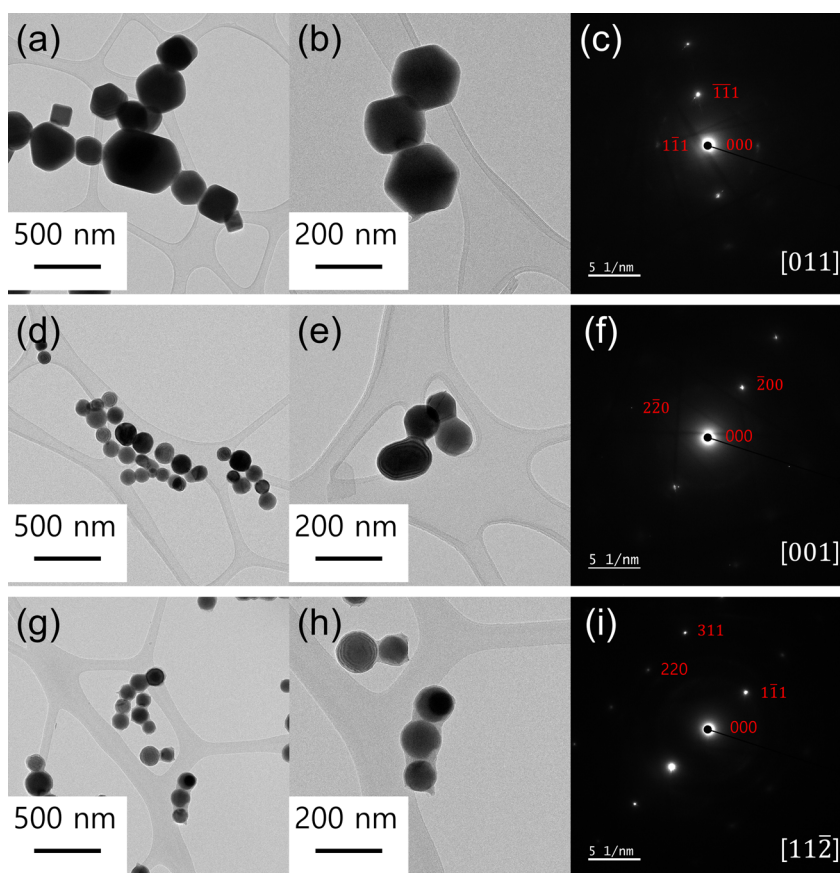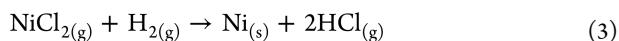
Figure 2. HRTEM images and SAED patterns of Ni-NPs synthesized in the CVS reactor using different precursors; (a–c) $NiCl_2$, (d–f) $NiSO_4$-mixed $NiCl_2$, and (g–i) Na_2SO_4-mixed $NiCl_2$.
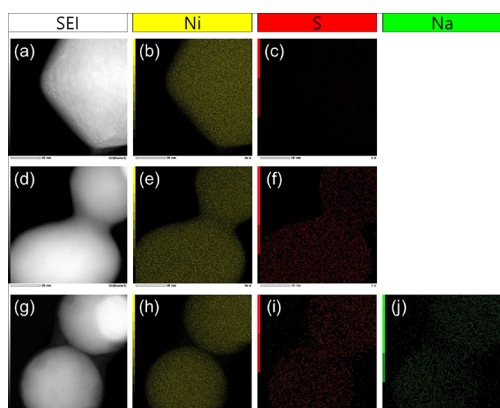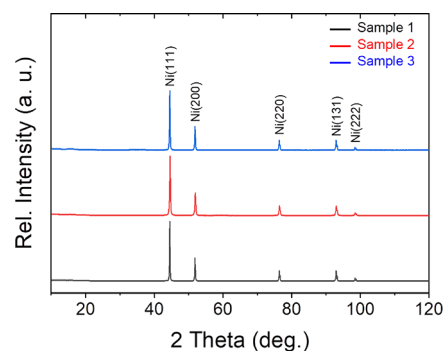

Figure 3. EDS mapping of Ni-NPs synthesized in the CVS reactor using different precursors; (a–c) $NiCl_2$, (d–f) $NiSO_4$-mixed $NiCl_2$, and (g–j) Na_2SO_4-mixed $NiCl_2$.

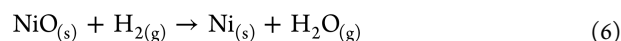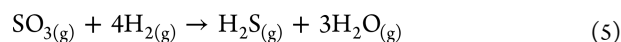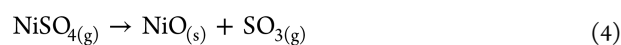**Figure 4.** XRD patterns of Ni-NPs synthesized by CVS using different precursors.

To explain what occurs when two different additives are inserted into the CVS reactor with $NiCl_2$ in a reducing atmosphere, all possible chemical reactions involved during the synthesis of Ni-NPs are written as follows. In the conventional reduction process, $NiCl_2$ reacts with H_2 to form Ni and HCl gases (eq 3).
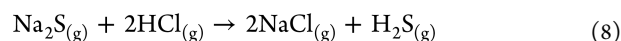
$$NiCl_{2(g)} + H_{2(g)} \rightarrow Ni_{(s)} + 2HCl_{(g)} \tag{3}$$

In the presence of $NiSO_4$, it undergoes several chemical reactions, as follows (eqs 4–6).

$$NiSO_{4(g)} \rightarrow NiO_{(s)} + SO_{3(g)} \tag{4}$$

$$SO_{3(g)} + 4H_{2(g)} \rightarrow H_2S_{(g)} + 3H_2O_{(g)} \tag{5}$$

$$NiO_{(s)} + H_{2(g)} \rightarrow Ni_{(s)} + H_2O_{(g)} \tag{6}$$

In the presence of Na_2SO_4, several chemical reactions occur, as follows (eqs 7 and 8).

$$Na_2SO_{4(g)} + 4H_{2(g)} \rightarrow Na_2S_{(g)} + 4H_2O_{(g)} \tag{7}$$

$$Na_2S_{(g)} + 2HCl_{(g)} \rightarrow 2NaCl_{(g)} + H_2S_{(g)} \tag{8}$$
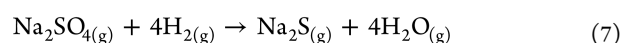
Following the above reactions (eqs 4–8), NiS is produced by the following reaction (eq 9).
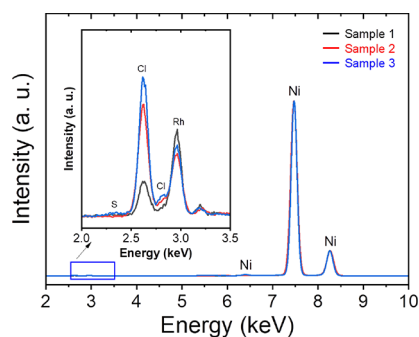
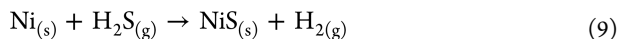**Figure 5.** XRF patterns of Ni-NPs synthesized by CVS using different precursors. (Inset) XRF data of S, Cl, and Na in the spectral region of 2.0−3.5 keV.

Table 3. Chemical Composition (wt %) of Samples 1−3

sample number	chemical composition			
	Ni	Cl	S	Na
1	99.60	0.40		
2	98.65	1.33	0.03	
3	98.27	1.72	0.01	0

$$Ni_{(s)} + H_2S_{(g)} \rightarrow NiS_{(s)} + H_{2(g)} \tag{9}$$

The values of the change in Gibbs free energy with temperature for each reaction (eqs 3−9) are presented in Figure 6. According to the Gibbs free energy calculations, all reactions discussed have negative values of the Gibbs energy change and are spontaneous reactions.
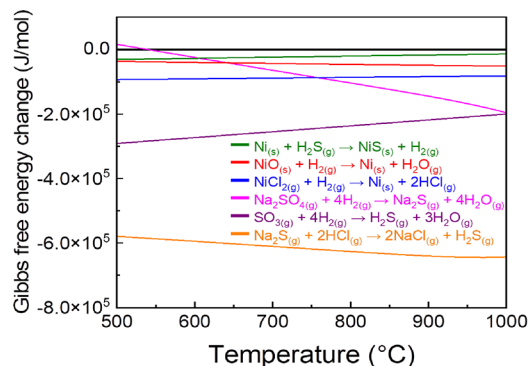

Figure 6. Values of the Gibbs free energy change with temperature for each reaction.

We calculated the surface energy of different facets for total surface coverages up to 0.5 ML, which is sufficient to observe the distinct effects of S addition on the change in Ni surface energy. Two planes with low Miller indices, Ni(100) and Ni(111), were modeled to observe the changes in the surface energies for the various surface coverages of Ni, Cl, and S species because these two facets mostly equilibrate the Ni-NPs.[32] Note that when surface energies with different structures become similar, the exposure preference for a particular surface diminishes, resulting in the formation of spherical particles. Although the surface energy of a high-index Ni plane can provide insight into the particle shape change, we adopted the most representative and plausible surfaces, Ni(100) and Ni(111), to be exposed. This is to simplify the phenomenon that different types of adsorbates vary the point

where surface energies become similar. Surface energies for Ni(100) and Ni(111) were initially calculated without any adsorbates and were found to have the values $\gamma_{100} = 2.08$ J/m^2 and $\gamma_{111} = 1.91$ J/m^2. These results are consistent with those obtained in most previous studies.[33]

The surface energies of the adsorbates were calculated assuming that the adsorbate−adsorbate interactions were identical among the adsorbates. For instance, the simultaneous adsorption of Ni and Cl with a coverage of 0.0625 ML each was considered as 0.125 ML in total. Changes in the surface energy as a function of coverage are shown in Figure 7.
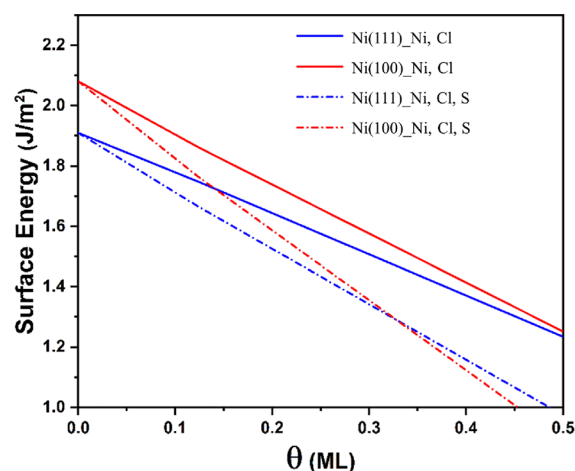
Figure 7. Effect of adsorbate species on the surface energy of Ni(111) and Ni(100) as a function of surface coverage (θ).

The surface energies of Ni(100) and Ni(111) decreased with the adsorbate coverage for all cases; however, the addition of S made the slope steeper. In particular, the Ni(100) surface energy was more sensitive to adsorption and crossed the Ni(111) line. In the case of S addition, the point at which Ni(111) and Ni(100) crossed appeared at a lower surface coverage, suggesting isotropic growth of the Ni surface; furthermore, the formation of spherical particles was easy in the presence of S.

The aforementioned DFT calculations indicate that S plays an important role in lowering the surface energy of the crystal facets to form spherical Ni-NPs.

4. CONCLUSIONS

Spherical Ni-NPs were prepared using $NiSO_4$-mixed $NiCl_2$ and Na_2SO_4-mixed $NiCl_2$ precursors in a CVS reactor. The shape change from faceted to spherical Ni-NPs occurred due to the presence of S atoms, which were identified to be the major contributing factor. The results of first-principles calculations indicated that the added S atom stabilizes Ni (hkl) more than Cl. This concept may help fabricate other spherical NPs using S impurities in the CVS reactor. This study provides a new route for changing the shape and size of Ni-NPs using $NiCl_2$ with an added S content.

■ ASSOCIATED CONTENT

Ⓢ Supporting Information

The Supporting Information is available free of charge at https://pubs.acs.org/doi/10.1021/acsomega.2c05281.

Additional experimental details, materials, and methods, including photographs of the experimental setup (PDF)

■ AUTHOR INFORMATION

Corresponding Authors

Seok Ki Kim — *Department of Chemical Engineering, Ajou University, Suwon, Gyeonggi-do 16499, Republic of Korea;* ⊙ orcid.org/0000-0002-6447-8287; Email: seokki@ajou.ac.kr

Young Keun Kim — *Department of Materials Science and Engineering, Korea University, Seoul 02841, Republic of Korea;* ⊙ orcid.org/0000-0002-0868-4625; Email: ykim97@korea.ac.kr

Seung-Min Yang — *Functional Materials and Components R&D Group, Korea Institute of Industrial Technology, Gangneung, Gangwon-do 25440, Republic of Korea;* ⊙ orcid.org/0000-0001-9346-5023; Email: ysm@kitech.re.kr

Authors

Yong-Su Jo — *Functional Materials and Components R&D Group, Korea Institute of Industrial Technology, Gangneung, Gangwon-do 25440, Republic of Korea; Department of Materials Science and Engineering, Korea University, Seoul 02841, Republic of Korea*

Mansurbek Abdullaev — *Korea Research Institute of Chemical Technology, Daejeon 34114, Republic of Korea*

Gwang-Hwa Jin — *Functional Materials and Components R&D Group, Korea Institute of Industrial Technology, Gangneung, Gangwon-do 25440, Republic of Korea; Department of Materials Science and Engineering, Korea University, Seoul 02841, Republic of Korea*

Bhabani Sankar Swain — *Functional Materials and Components R&D Group, Korea Institute of Industrial Technology, Gangneung, Gangwon-do 25440, Republic of Korea*

Byongpil Lee — *Rare Metals Cell Group, Research Institute of Industrial Science & Technology, Pohang, Gyeongsangbukdo 37673, Republic of Korea*

Hyung-Sub Eom — *Rare Metals Cell Group, Research Institute of Industrial Science & Technology, Pohang, Gyeongsangbukdo 37673, Republic of Korea*

Seok-Hong Min — *Korea Institute of Industrial Technology Interdisciplinary Program, Gangneung-Wonju National University, Gangneung, Gangwon-do 25457, Republic of Korea*

Complete contact information is available at:
https://pubs.acs.org/10.1021/acsomega.2c05281

Notes

The authors declare no competing financial interest.

■ ACKNOWLEDGMENTS

■ REFERENCES

(1) Im, T.; Pyo, J.; Lee, J.-S.; Lee, C. S. Fabrication of homogeneous nanosized nickel powders using a planetary ball mill: Applications to multilayer ceramic capacitors (MLCCs). *Powder Technol.* **2021**, *382*, 118−125.

(2) Songping, W. Preparation of ultra fine nickel−copper bimetallic powder for BME-MLCC. *Microelectron. J.* **2007**, *38*, 41−46.

(3) Wang, A.; Yin, H.; Lu, H.; Xue, J.; Ren, M.; Jiang, T. Effect of organic modifiers on the structure of nickel nanoparticles and catalytic activity in the hydrogenation of p-nitrophenol to p-aminophenol. *Langmuir* **2009**, *25*, 12736−12741.

(4) Wang, H. Y.; Lua, A. C. Development of metallic nickel nanoparticle catalyst for the decomposition of methane into hydrogen and carbon nanofibers. *J. Phys. Chem. C* **2012**, *116*, 26765−26775.

(5) Oh, Y. J.; Kim, J. H.; Park, S.-K.; Park, J.-S.; Lee, J.-K.; Kang, Y. C. Highly efficient hierarchical multiroom-structured molybdenum carbide/carbon composite microspheres grafted with nickel-nano-particle-embedded nitrogen-doped carbon nanotubes as air electrode for lithium-oxygen batteries. *Chem. Eng. J.* **2018**, *351*, 886−896.

(6) Zhong, G.; Li, S.; Xu, S.; Liao, W.; Fu, X.; Peng, F. Nickel nanoparticles encapsulated in nitrogen-doped carbon nanotubes as excellent bifunctional oxygen electrode for fuel cell and metal-air battery. *ACS Sustainable Chem. Eng.* **2018**, *6*, 15108−15118.

(7) Jiang, Y.; Zhou, C.; Liu, J. A non-polarity flexible asymmetric supercapacitor with nickel nanoparticle@ carbon nanotube three-dimensional network electrodes. *Energy Storage Mater.* **2018**, *11*, 75−82.

(8) Wu, X.; Xing, W.; Zhang, L.; Zhuo, S.; Zhou, J.; Wang, G.; Qiao, S. Nickel nanoparticles prepared by hydrazine hydrate reduction and their application in supercapacitor. *Powder Technol.* **2012**, *224*, 162−167.

(9) Kolhatkar, A.; Jamison, A.; Litvinov, D.; Willson, R.; Lee, T. Tuning the magnetic properties of nanoparticles. *Int. J. Mol. Sci.* **2013**, *14*, 15977−16009.

(10) Mostafa, S.; Behafarid, F.; Croy, J. R.; Ono, L. K.; Li, L.; Yang, J. C.; Frenkel, A. I.; Cuenya, B. R. Shape-dependent catalytic properties of Pt nanoparticles. *J. Am. Chem. Soc.* **2010**, *132*, 15714−15719.

(11) Fraige, F. Y.; Langston, P. A.; Chen, G. Z. Distinct element modelling of cubic particle packing and flow. *Powder Technol.* **2008**, *186*, 224−240.

(12) Yang, M.; Zhu, H.; Zheng, Y.; Zhang, C.; Luo, G.; Xu, Q.; Li, Q.; Zhang, S.; Goto, T.; Tu, R. One-step chemical vapor deposition fabrication of Ni@NiO@graphite nanoparticles for the oxygen evolution reaction of water splitting. *RSC Adv.* **2022**, *12*, 10496−10503.

(13) Gao, W.; Shen, S.; Cheng, Y. Synthesis of dispersed superfine FCC nickel single crystals in gas phase. *J. Phys. Chem. C* **2013**, *117*, 9223−9228.

(14) Yang, S.-M.; Kim, D.-S.; Choi, H.; Kim, K.-H.; Hwang, N.-M. Shape change of submicron nickel particles under hydrogen and nickel chloride vapor. *Appl. Surf. Sci.* **2020**, *509*, No. 145274.

(15) Jo, Y.-S.; Lee, H.-J.; Park, H.-M.; Na, T.-W.; Jung, J.-S.; Min, S.-H.; Kim, Y. K.; Yang, S.-M. Chemical Vapor Synthesis of Nonagglomerated Nickel Nanoparticles by In-Flight Coating. *Omega* **2021**, *6*, 27842−27850.

(16) Malekzadeh, M.; Swihart, M. T. Vapor-phase production of nanomaterials. *Chem. Soc. Rev.* **2021**, *50*, 7132−7249.

(17) Jung, D.-W.; Oh, S.-M.; Park, D.-W. Preparation of nickel nanopowder using the transferred arc plasma for MLCCs. *Korean Chem. Eng. Res.* **2008**, *46*, 701−706.

(18) Bai, L.; Fan, J.; Hu, P.; Yuan, F.; Li, J.; Tang, Q. RF plasma synthesis of nickel nanopowders via hydrogen reduction of nickel hydroxide/carbonate. *J. Alloys Compd.* **2009**, *481*, 563−567.

(19) Hong, J.-S.; Jo, W.; Ko, K.-J.; Hwang, N. M.; Kim, D.-Y. Equilibrium shape of nickel crystal. *Philos. Mag.* **2009**, *89*, 2989−2999.

(20) Meltzman, H.; Chatain, D.; Avizemer, D.; Besmann, T. M.; Kaplan, W. D. The equilibrium crystal shape of nickel. *Acta Mater.* **2011**, *59*, 3473−3483.

(21) Sidhaye, D. S.; Bala, T.; Srinath, S.; Srikanth, H.; Poddar, P.; Sastry, M.; Prasad, B. L. V. Preparation of nearly monodisperse nickel nanoparticles by a facile solution based methodology and their ordered assemblies. *J. Phys. Chem. C* **2009**, *113*, 3426−3429.

(22) Vakil, P. N.; Hardy, D. A.; Strouse, G. F. Synthesis of highly uniform nickel multipods with tunable aspect ratio by microwave power control. *ACS Nano* **2018**, *12*, 6784−6793.

(23) Lakhapatri, S. L.; Abraham, M. A. Sulfur poisoning of Rh−Ni catalysts during steam reforming of sulfur-containing liquid fuels. *Catal. Sci. Technol.* **2013**, *3*, 2755−2760.

(24) Yoneima, T.; Fukushima, K.; Saito, N.; Nakashima, K. Effect of sulfur on the sintering of nickel particles. *Mater. Trans.* **2016**, *57*, 1374−1377.

(25) Sehested, J. Four challenges for nickel steam-reforming catalysts. *Catal. Today* **2006**, *111*, 103−110.

(26) Ko, C. H.; Park, J. G.; Park, J. C.; Song, H.; Han, S.-S.; Kim, J. N. Surface status and size influences of nickel nanoparticles on sulfur compound adsorption. *Appl. Surf. Sci.* **2007**, *253*, 5864−5867.

(27) Kresse, G.; Joubert, D. From ultrasoft pseudopotentials to the projector augmented-wave method. *Phys. Rev. B* **1999**, *59*, 1758−1775.

(28) Kresse, G.; Furthmüller, J. Efficiency of ab-initio total energy calculations for metals and semiconductors using a plane-wave basis set. *Comput. Mater. Sci.* **1996**, *6*, 15−50.

(29) Kresse, G.; Furthmüller, J. Efficient iterative schemes for *ab initio* total-energy calculations using a plane-wave basis set. *Phys. Rev. B* **1996**, *54*, 11169−11186.

(30) Perdew, J. P.; Burke, K.; Ernzerhof, M. Generalized gradient approximation made simple. *Phys. Rev. Lett.* **1996**, *77*, 3865−3868.

(31) Pederson, M. R.; Ruzsinszky, A.; Perdew, J. P. Communication: Self-interaction correction with unitary invariance in density functional theory. *J. Chem. Phys.* **2014**, *140*, 121103.

(32) Zhang, W.-B.; Chen, C.; Zhang, S.-Y. Equilibrium crystal shape of Ni from first principles. *J. Phys. Chem. C* **2013**, *117*, 21274−21280.

(33) Tran, R.; Xu, Z.; Radhakrishnan, B.; Winston, D.; Sun, W.; Persson, K. A.; Ong, S. P. Surface energies of elemental crystals. *Sci. Data* **2016**, *3*, 160080.